Supplement of Atmos. Chem. Phys., 24, 9597–9614, 2024
https://doi.org/10.5194/acp-24-9597-2024-supplement

Atmospheric Chemistry and Physics
Open Access
EGU

Supplement of

Aerosol optical properties within the atmospheric boundary layer predicted from ground-based observations compared to Raman lidar retrievals during RITA-2021

Xinya Liu et al.

Correspondence to: Xinya Liu (xinya.liu@rug.nl) and Ulrike Dusek (u.dusek@rug.nl)

S1 Merged particle size distribution

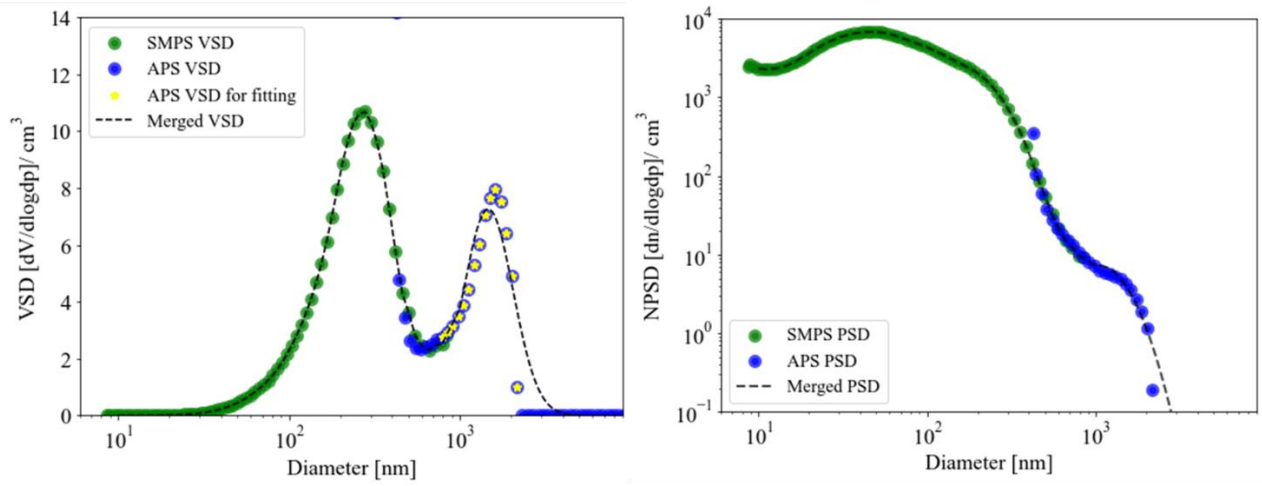

Figure S1: Example of the joined particle size distribution. (a) The volume size distribution (VSD) (dv/dlog(dp) cm^{-3}) of raw MPSS data (green dots). The VSD of APS data (blue dots). The selected APS data for fitting (yellow stars). The final joined VSD with dash line. (b) The PSD (particle number size distribution) (dn/dlogdp cm^{-3}) of MPSS (green dots), and the PSD of APS (blue dots), as well as the joined PSD (dash line).

Figure S1 shows an example of the merged particle size distribution by the MPSS and APS. The APS aerodynamic diameters were converted to volume equivalent diameters by dividing by the square root of particle effective density. The effective density was derived by an iterative approach. The volume size distribution for coarse particles (greater than 2.5 micrometres aerodynamic diameter) is converted to a mass size distribution assuming various effective densities spanning from 1.0 to 2.0 ($g \cdot cm^{-3}$), with steps of 0.1. Each obtained mass distribution is then integrated to compute the total mass concentration of coarse particles. The calculated coarse mass concentrations for each assumed density are then compared to the measured coarse mode mass concentrations, determined as the difference between PM_{10} and $PM_{2.5}$ mass concentrations from gravimetric analysis. The effective density for each case is the density for which the calculated and measured coarse mode mass concentrations agree best. The average effective density is 1.6 $g \cdot cm^{-3}$. For missing or unrealistic APS data, showing a sudden drop to 0 (see figure S1(a)) or negative values or unrealistically high values, it was assumed that the coarse mode volume size distribution follows a lognormal distribution. The mean and standard deviation of the coarse mode was then fixed based on the coarse mode distributions that were measured during earlier Trolix campaigns in 2019. Then the lognormal distribution fitting and interpolation were performed on the obtained particle size distribution data (as shown in Figure S1). An average $\mu = 7.70 \pm 0.14$ and $\sigma = 0.46 \pm 0.05$ were used in the correction for the wrong APS data with fitting equation as below:

$$f(x) = \frac{1}{x\sigma\sqrt{2\pi}} \exp\left(-\frac{(\ln x - \mu)^2}{2\sigma^2}\right),$$

where the x is the diameter (nm), the yellow point in FigureS1 in this case. The μ is the mean of samples in distribution, and σ is the standard deviation, both on the log-scale.

S2 Additional profiles for compression between the modelling and Raman lidar

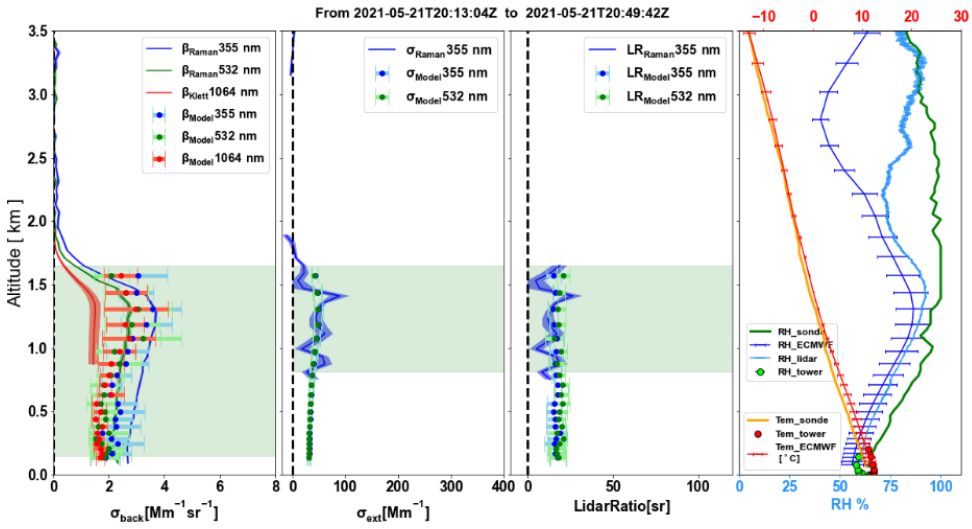

Figure S 2: Profiles from 20:13 to 20:49 at UTC time on 2021-05-21.

Figure S2 presents a particularly clear example from a marine air mass. A very low $PM_{2.5}$ mass concentration with an average of 0.89 ± 0.07 µg m^{-3} was observed during this period, with a chloride mass fraction of 5.1% (usually less than 1%), possibly indicating the presence of other chlorine-rich, inorganic salt particles from the sea. The trends in lidar measured backscatter coefficient profiles and RH profiles demonstrate good agreement, indicating that the increase in the backscatter coefficient with altitude is primarily influenced by RH. However, model results exhibit large uncertainties due to very low aerosol concentrations. Nevertheless, the extinction coefficients and lidar ratio, display good consistency between 1 and 1.4 km.

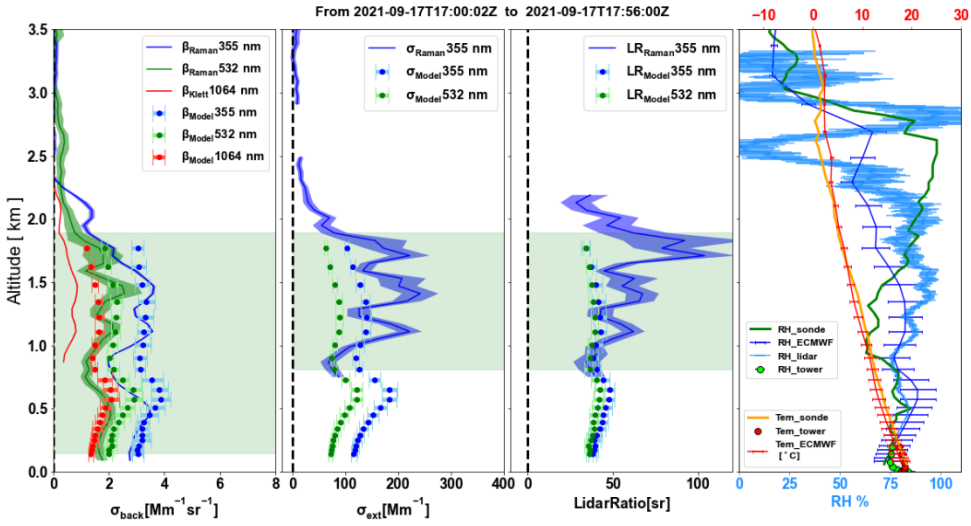

Figure S3: Profiles from 17:00 to 17:56 at UTC time on 2021-09-17.

In contrast, Figure S3 shows a case characterized by higher contamination, with an average mass concentration of 11.39 ± 1.26 µg m^{-3}. The model shows good agreement with the lidar measured results across the entire vertical profiles

of the backscatter coefficient, especially in the region below 500 meters. For the extinction coefficient and lidar ratio profiles, values observed above 1 km could most likely indicate variations in aerosol distribution, or they may also slightly reflect the model's limitations to capture these changes due to insufficient vertical resolution accuracy of RH profiles. Nevertheless, the results stayed within an acceptable range.

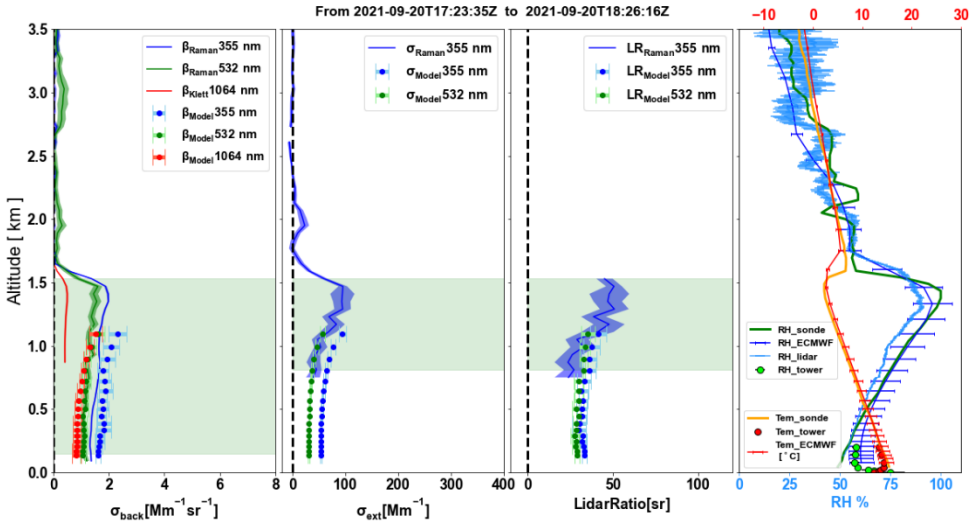

Figure S4: Profiles from 17:23 to 18:26 at UTC time on 2021-09-20.

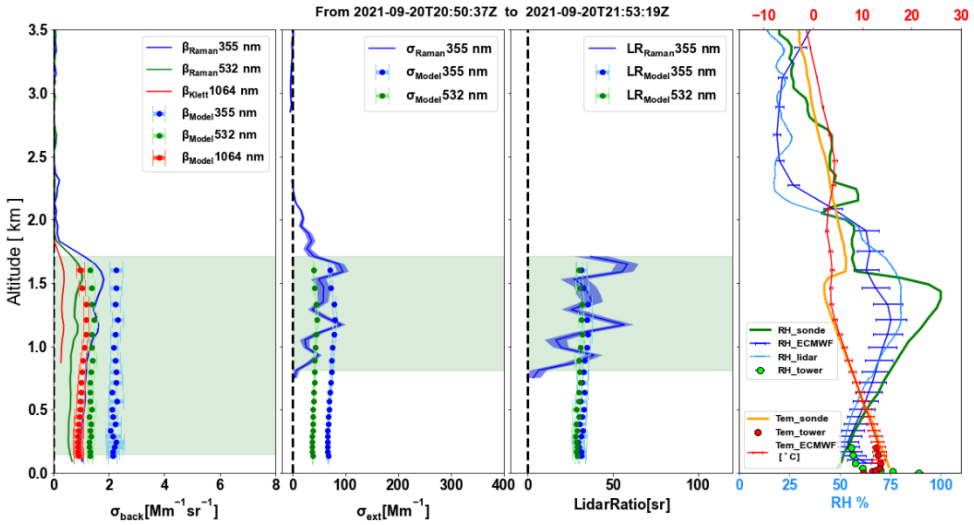

Figure S5: Profiles from 20:50 to 21:53 at UTC time on 2021-09-20.

Figures 4 and 5 show the results of two different time periods (from 17:23 to 18:26 and from 20:50 to 21:53) on the day 2021-09-20. In the earlier period, the model results aligned closely with the lidar observations. However, during the later period, the model significantly overestimated the backscatter coefficient, with estimations one times higher than the lidar measurements. This discrepancy is primarily attributed to the night-time increase of aerosol concentration at the ground from the earlier to the later time period (from 6.96 ± 1.15 µg m^{-3} to 9.25 ± 0.41 µg m^{-3}). This elevation in aerosol levels leads the model to overestimate both the backscattering and extinction coefficients. However, the simulation of the lidar ratio remains reasonable.

Table S1: The scattering coefficient and backscatter coefficient comparison between nephelometer measurements and calculations by assuming all sea salt (SS) or mineral dust (MD) in coarse mode.

SS coarse mode	Scattering coeffcient			backscattering coefficient		
Wavelength (nm)	450	550	700	450	550	700
Slope	0.84	0.95	0.95	1.00	1.17	1.09
R^2	0.90	0.91	0.92	0.65	0.75	0.68
Intercept	-1.30E-06	-3.40E-06	-6.20E-06	1.30E-06	3.10E-08	-2.50E-07
MD coarse mode	Scattering coeffcient			backscattering coefficient		
Wavelength (nm)	450	550	700	450	550	700
Slope	0.84	0.94	0.95	1.11	1.20	1.12
R^2	0.90	0.91	0.91	0.68	0.65	0.74
Intercept	-1.80E-06	-3.70E-06	-6.60E-06	2.80E-07	8.90E-07	-7.90E-07

S3 The estimation of the Mineral Dust and Sea Salt

As the coarse mode chemical composition was not measured during the RITA campaign, we made use of the measurements obtained from the previous Trolix campaign in 2019.

Sea salt (SS) aerosols are prominently found in the atmosphere over the Netherlands. They originate from seawater, which is entrained into the atmosphere by breaking waves and spumes. Hence, the composition of pure sea salt aerosol reflects that of sea water, encompassing natural organic compounds and pollutants. In this research, sodium serves as the ideal tracer because it offers the advantage of minimal losses due to depletion, ensuring reliable measurements. The recovery rate for sodium prior to analysis using ICP-MS stands at 100%, guaranteeing dependable detections. Conversely, when considering chloride, atmospheric reactions may lead to interactions with sulfuric and nitric acids, potentially resulting in the depletion of Cl^- ions within the aerosol. As such, the presence of SS was estimated based on:

$SS = 3.26 * [Na^+]$.

Where the factor 3.26 stems from the relative mass contribution of Na in North Sea water. This approach is adopted from Schaap et al (2010).

Mineral Dust (MD) is also part of the atmospheric aerosol mixture in the Netherlands(Denier van der Gon et al., 2010). Silicon (Si) and Aluminum (Al) have been identified as promising tracers for MD analysis, but both element analyses suffer from recovery issues. In our analyses, the Silicon was biased low (40% recovery) in the analysis because in the open destruction step with HF, SiF_4 is evaporated. In contrast, Al exhibited a considerably higher recovery rate, approximately 70%. Given the superior recovery rate of Al, we have opted to utilize Al elemental analyses as the basis for estimating atmospheric MD concentrations (Hendriks et al., 2008; Denier van der Gon et al., 2010). We correct the Al concentration for unrecovered material by division with 0.70. As SiO_2 and Al_2O_3 are the most abundant minerals for Si and Al, respectively, we represent the entire mixture as follows:

[Al-based mass] = [Al] * (1 + 1.5 * (M-O/M-Al)), where M-O = 16.0 and M-Al = 27.0

[Si-based mass] = [Si] * (1 + 2 * (M-O/M-Si)), where M-Si = 28.1

It's important to note that the MD mass estimated using Al and Si as tracers typically serves as a conservative estimate, representing a lower limit of the total MD mass. Then the volume concentration of the SS and MD can be obtained by dividing their mass concentrations by the corresponding densities, and those parameters are listed in Table 1.

References

Denier van der Gon, H., Jozwicka, M., Hendriks, E., Gondwe, M., and Schaap, M.: Mineral Dust as a component of particulate matter, PBL Netherlands Environ. Assesment Agency, 160, 2010.

Hendriks, E. C. J., Gon, H. A. C. D. Van Der, and Schaap, M.: Constraining the potential source strength of various soil dust sources contributing to atmospheric PM10 concentrations in Europe, 80015, 2008.

Schaap, M., Weijers, E. ., Mooibroek, D., Nguyen, L., and Hoogerbrugge, R.: Composition and origin of particulate matter in the Netherlands, RIVM Rapp., 69, 2010.